

Research Paper

Thermo- and pH-dual responsive polymeric micelles with upper critical solution temperature behavior for photoacoustic imaging-guided synergistic chemo-photothermal therapy against subcutaneous and metastatic breast tumors

Zhe Yang^{1,*}, Rui Cheng^{1,*}, Chenyang Zhao¹, Na Sun¹, Huiyan Luo³, Ya Chen³, Zerong Liu¹, Xian Li¹, Jie Liu^{2,✉}, Zhongmin Tian^{1,✉}

1. The Key Laboratory of Biomedical Information Engineering of Ministry of Education, School of Life Science and Technology, Xi'an Jiaotong University, Xi'an 710049, China
2. Department of Biomedical Engineering, School of Engineering, Sun Yat-sen University, Guangzhou 510006, China
3. Department of Medical Oncology, Sun Yat-sen University Cancer Center; State Key Laboratory of Oncology in South China, Guangzhou 510060, China

* These authors contribute equally to this work.

✉ Corresponding author: E-mail: liujie56@mail.sysu.edu.cn; zmtian@xjtu.edu.cn. Tel: 0086-20-3933-2145; 0086-29-82667331

© Ivyspring International Publisher. This is an open access article distributed under the terms of the Creative Commons Attribution (CC BY-NC) license (<https://creativecommons.org/licenses/by-nc/4.0/>). See <http://ivyspring.com/terms> for full terms and conditions.

Received: 2018.03.20; Accepted: 2018.06.20; Published: 2018.07.16

Abstract

Chemo-photothermal therapy shows great potential for inhibiting tumor growth. However, achieving maximal chemo-photothermal synergistic efficacy is challenging because of the low efficiency of controllable chemo-drug release in response to external or internal triggers. Thus, a nano-delivery system that could effectively achieve photothermal therapy and dual stimuli-responsive (heat and pH) drug release to inhibit both primary breast tumor growth and metastases is required.

Methods: Herein, a thermo- and pH-responsive polymer (mPEG-PAAV) with an upper critical solution temperature (UCST) was synthesized to fabricate a DOX- and IR780-loaded micellar system. After systematic studies of the photothermal performance and controllable drug release of mPEG-PAAV micelles/IR780+DOX under NIR irradiation at different pH values, their chemo-photothermal synergistic therapy efficacies were also estimated both *in vitro* and *in vivo*.

Results: Because of the photothermal conversion of mPEG-PAAV micelle/IR780+DOX (~200 nm, 3.82 mV), high local temperature could be induced at the tumor site under NIR laser irradiation. This hyperthermia not only produced an enhanced tumor necrosis, but also broke down the micelles under the decreased pH environment, resulting in rapid DOX release and enhanced intracellular drug accumulation after NIR laser irradiation. In addition, photoacoustic imaging (PAI) of mPEG-PAAV/IR780+DOX micelle was adopted to monitor the morphology and micro-vascular distribution of the tumor tissue, which could also guide the chemo-photothermal therapy. Most importantly, the systemic administration of mPEG-PAAV micelles/IR780+DOX combined with NIR laser irradiation could simultaneously eliminate the 4T1 breast tumor and thoroughly suppress lung metastasis without any obvious adverse effects.

Conclusion: Herein, a pH- and thermo-dual responsive UCST micelle system was developed for delivering IR780 and DOX, which could achieve NIR laser-controlled drug release and PA imaging guidance for chemo-photothermal synergistic therapy of both primary breast tumors and their metastases.

Key words: upper critical solution temperature (UCST), chemo-photothermal therapy, controlled release, photoacoustic imaging, breast cancer

Introduction

Breast cancer, with its high chance of metastasis, is the major cause of cancer-related death among women, with more than one million cases being newly diagnosed annually worldwide [1]. The overall 5-year survival rate of breast cancer patients is only 10% because of metastasis and recurrence [2, 3]. Therefore, it is necessary to find an approach that could simultaneously inhibit breast tumor growth and metastasis.

The development of nanomedicines has been a milestone in cancer therapy, many of which have been used in the clinic for chemotherapy, gene therapy, radiotherapy, immunotherapy and photothermal therapy (PTT) [4]. Recently, due to its minimized invasiveness, better preservation of surrounding tissues and lower complication rates, NIR laser-mediated PTT has attracted increased attention as an emerging strategy for breast cancer treatment [5, 6]. The hyperthermia effect induced by PTT can not only accelerate the cellular uptake of chemotherapeutics but also enhance the cytotoxicity of chemotherapeutics *in vitro* and *in vivo* [7-10]. Moreover, many studies have already confirmed that the combination of PTT and chemotherapy is able to effectively suppress the spread of metastatic breast tumors into lungs [11-13]. For instance, Zhuang Liu et al. prepared a multifunctional "Abraxane-like" nano-drug consisting of paclitaxel (PTX) for chemotherapy and indocyanine green (ICG) for PTT, which eradicated subcutaneous tumors, resulting in significant therapeutic benefits for mice with metastatic tumors [11]. Unfortunately, their further applications were still limited by other challenges [6]: the *ex-vivo* NIR laser failed to effectively realize controllable drug release, which prevented the chemotherapeutic drug and photothermal agent from simultaneously exerting their synergistic effect properly.

Facing such challenges, intelligent and environmental-responsive nano-systems with NIR light-controllable drug release become extremely important for chemo-photothermal therapy. In these stimuli-responsive nano-delivery systems, the structure is lost or destroyed under one or two stimuli, such as temperature, light, enzymes or pH [14]. Among all stimuli-responsive nano-delivery systems, pH-sensitive and thermo-sensitive polymeric delivery systems are suitable for chemo-photothermal therapy because they can exploit the acidic condition of solid tumors and the hyperthermia induced by PTT to achieve controlled drug release. Firstly, the differences in pH values between normal tissue/blood and tumor extracellular environment are intrinsic and simple, and such characteristics have been widely used in drug delivery systems for

controlled drug release [15, 16]. Additionally, thermo-sensitive polymeric delivery systems with an upper critical solution temperature (UCST) can be precisely controlled by temperature [17-20]. For example, below UCST, polymers contact each other through intermolecular interactions and form stiff particles to prevent drug leakage; conversely, the intermolecular interactions are broken at temperatures above UCST, resulting in disassembly of the particles and rapid drug release [21]. So, combining a UCST micellar delivery system with a photothermal strategy could maximize instantaneous drug release and promote the therapeutic effect [22].

Herein, an amphiphilic polymer, poly(ethylene glycol)-*b*-poly(acrylamide-*co*-acrylonitrile-*co*-vinylimidazole) copolymer (mPEG-PAAV), was synthesized, the UCST of which is automatically changed at different pH values. In order to realize NIR laser-controlled drug release, mPEG-PAAV copolymer was employed to create a DOX- and IR780-loaded micellar system (**Figure 1**). IR780, as a NIR absorber, can effectively convert NIR laser energy into heat [23, 24], triggering DOX release from mPEG-PAAV micelle. Additionally, IR780 can be used for PAI because of its strong NIR absorption peak. This can help in guiding the chemo-photothermal therapy and monitoring the tumor morphology and microvascular distribution *in vivo* [25]. To examine whether this intelligent micellar system could be an effective platform to realize NIR laser-controlled drug release and PAI-guided chemo-photothermal therapy against subcutaneous and metastatic breast tumor, we studied its characteristics, such as: thermo- and pH-responsiveness, photothermal conversion efficiency, drug release, cellular uptake, and *in vitro* therapeutic efficiency. In addition, 4T1 tumor-bearing mice were used to estimate their tumor targeting capacity, antitumor efficacy, and biosafety.

Methods

Materials, cells and animals

1-Vinylimidazole (VIm), acrylonitrile (AN), acrylamide (AAm), 2, 2'-azoisobutyronitrile (AIBN), N-(3-dimethylaminopropyl)-N'-ethylcarbodiimide hydrochloride (EDC), Hoechst 33342, IR780, N-hydroxysuccinimide (NHS), 2-aminoethanethiol hydrochloride (AET·HCl), 9,10-anthracenediyl-bis(methylene) dimalonic acid (ABDA) and MTT were obtained from Sigma. Methoxy poly(ethylene glycol) carboxyl acid (mPEG-COOH, 5 kDa) was obtained from Yare Bio-Technology Co. Ltd. (China). DOX was obtained from Beijing Huafeng United Technology Co., Ltd. (China).

The protocol for animal experiments was approved by the Animal Experimentation Ethics

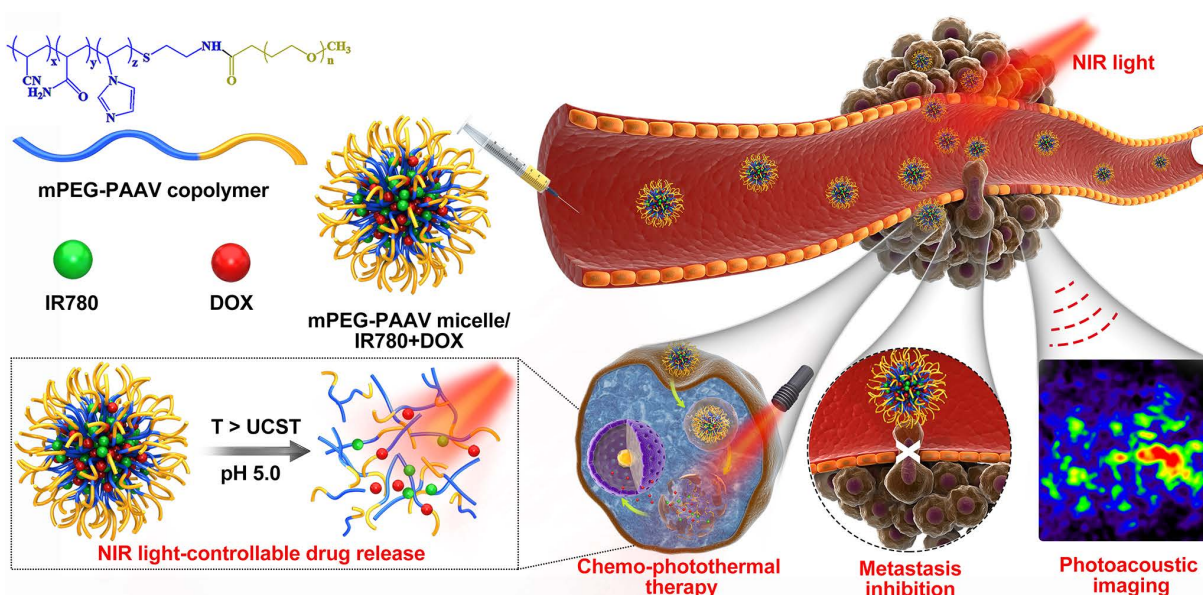


Figure 1. Schematic illustration of the chemo-photothermal therapy of IR780- and DOX-loaded mPEG-PAAV micelle with NIR laser-controlled drug release.

Committee of Xi'an Jiaotong University. In order to obtain mice bearing 4T1 tumors, approximately 1×10^6 4T1 cells (murine breast cancer cells) were inoculated subcutaneously into the flank of female balb/c mice (4 weeks old). The length and width of tumor were measured and the following formula was employed to calculate the tumor volume: volume = $0.5 \times \text{width}^2 \times \text{length}$.

Synthesis of PAAV copolymer

The P(AAm-co-AN-co-VIm) copolymer (PAAV) was synthesized *via* radical polymerization using AIBN as initiator and AET·HCl as chain transfer agent [26]. In brief, AET·HCl, AIBN, 1-vinylimidazole, acrylonitrile and acrylamide, were co-dissolved in 10 mL of anhydrous dimethylformamide (DMF) and added into a 25 mL Schlenk flask under argon flow. The mixture solution was degassed *via* freeze-vacuum-thaw cycles three times and reacted at 65 °C under argon for 24 h. Afterwards, the reaction solution was precipitated in cold methanol. Subsequently, the resulted PAAV copolymer was dialyzed against deionized water and lyophilized for further use.

Synthesis of mPEG-PAAV copolymer

mPEG-COOH was chemically conjugated to PAAV copolymer by reacting the carboxyl end group of mPEG with the amino end group of PAAV. Briefly, mPEG-COOH and PAAV were co-dissolved in 10 mL of anhydrous DMF. Then, EDC (1.5 eq. molar of mPEG-COOH), NHS (1.5 eq. molar of mPEG-COOH) and triethylamine (TEA, 5 μ L) in anhydrous DMF were added into the reaction solution and then stirred at 35 °C overnight. After reaction, the resultant

polymer was precipitated in cold methanol, dialyzed against deionized water and lyophilized for further studies.

The chemical structure and the molecular weights of the resulted copolymers were characterized using ^1H NMR spectroscopy (Agilent Technologies 800/54 premium) and gel permeation chromatography (GPC, Waters), respectively.

Preparation and characterization of mPEG-PAAV micelles

In brief, the mPEG-PAAV copolymer was dissolved in dimethyl sulfoxide (DMSO) and injected into PBS (pH=7.4) under probe sonication at 14 W for 1 min on ice (Sonics & Materials, VCX500). The resultant micelles were then dialyzed against PBS overnight.

The size and zeta potential of mPEG-PAAV micelles were characterized using a dynamic light scattering (DLS) analyzer (NanoBrook 90Plus, USA). To examine the morphology of mPEG-PAAV micelles, the samples were dropped on a copper grid and negatively stained by phosphotungstic acid aqueous solution (0.2% w/w) for 30 s. Then, the staining solution was removed and a transmission electron microscope (TEM, JEM-200CX) was used to image the mPEG-PAAV micelles.

Stability of mPEG-PAAV micelles

With the aim to evaluate the stability of mPEG-PAAV micelles in physiological condition, the micelles were incubated in PBS (pH 7.4, 0.01 M) containing 10% FBS (v/v) at 37 °C for 48 h, and the size distributions of mPEG-PAAV micelles were measured during the incubation. Additionally, we

also measured the size distribution of mPEG-PAAV micelles at different temperature (25 °C, 45 °C, 65 °C) in PBS (pH 7.4, 0.01 M) containing 10% FBS (v/v).

Hemolysis and erythrocyte agglutination assay

To evaluate the hemocompatibility of mPEG-PAAV micelles, erythrocytes were collected and incubated with the micelles at different concentrations (50-400 µg/mL) at 37 °C for 24 h. PBS (pH 7.4, 0.01 M) and Triton X-100 (1%, v/v) solution were employed as negative and positive controls, respectively. The hemolysis induced by mPEG-PAAV micelles or control groups after 24 h incubation was characterized by measuring the concentration of the released hemoglobin, which was collected by centrifuging (402 g, 5 min) the above suspension. The hemolytic activity (%) of different groups was calculated using the following equation: Hemolysis (%) = $(A_{\text{Sample}} - A_{\text{PBS}}) / (A_{\text{Triton}} - A_{\text{PBS}}) \times 100\%$, where A_{Sample} , A_{PBS} and A_{Triton} represent the absorbance intensity of hemoglobin at 410 nm in mPEG-PAAV micelles, PBS and Triton X-100 groups, respectively. Additionally, the erythrocyte agglutination induced by each sample group was observed under a microscope.

In vitro cytotoxicity of blank mPEG-PAAV micelles

Briefly, 4T1 cells were used and incubated with blank mPEG-PAAV micelles at varying concentrations (50-400 µg/mL) for 48 h and then the *in vitro* cytotoxicity of mPEG-PAAV micelles was estimated using MTT assay.

Turbidity measurements

To measure the UCST of the copolymer, its turbidity in PBS at different pH values was recorded using a UV-Vis spectrophotometer (Purkinje T6-1610F, China) at a wavelength of 650 nm with a heating rate of 0.5 °C/min. UCST was defined as the temperature where the transmittance reached half of the maximum value during the whole heating process.

Preparation and characterization of mPEG-PAAV micelles/IR780+DOX

IR780- and DOX-loaded mPEG-PAAV micelles were fabricated using a similar protocol except that mPEG-PAAV copolymers, IR780 and DOX were co-dissolved in DMSO. The Fourier transform infrared (FT-IR, Nicolet™ iS50) and X-ray diffraction (XRD, Ultima IV) spectra of different samples were measured to confirm that DOX and IR780 were encapsulated in mPEG-PAAV micelles. For XRD measurements, samples were added to a quartz sample holder, and scanned over 2θ range (5–80 °) at a scan rate of 10 °/min.

The content of IR780 and DOX in mPEG-PAAV micelles was evaluated using fluorescence spectrometry (Hitachi F7000) at excitation wavelengths of 480 nm (DOX) and 740 nm (IR780), respectively. The drug loading and entrapment efficiency of mPEG-PAAV micelles/IR780+DOX were calculated using the following equations:

$$\text{Drug loading (\%)} = \frac{\text{drug amount in NPs}}{\text{mass of NPs}} \times 100\%$$

$$\text{Entrapment Efficiency (\%)} = \frac{\text{drug amount in NPs}}{\text{amount of drug used}} \times 100\%$$

NIR laser-induced temperature increase in vitro

To study the photothermal efficiency of mPEG-PAAV micelles/IR780+DOX, PBS, blank mPEG-PAAV micelles and other drug formulations at the same concentration of IR780 were exposed to NIR laser irradiation (808 nm, 3 W/cm²) for 400 s. The temperature change of each group was monitored using a digital thermometer. Moreover, the effects of IR780 concentration and laser power density on the photothermal efficiency of mPEG-PAAV micelles/IR780+DOX were also investigated.

Temperature- and pH-dependent drug release

mPEG-PAAV micelles/IR780+DOX in PBS (pH 7.4, 6.5 and 5.0) were added into dialysis bags against the same PBS at different temperatures (25 °C, 37 °C and 43 °C). The DOX released from the micelle samples at pre-determined time intervals was quantified using the fluorescence spectrometry method described above.

Laser-triggered drug release

To assess the photothermal release of DOX from mPEG-PAAV micelles at varying pH values (pH 5.0, 6.5 and 7.4), mPEG-PAAV micelles/IR780+DOX were either irradiated with NIR laser (808 nm, 3 W/cm², 5 min) three times, or left as controls. The following steps were the same as the procedures in the above section.

Inhibition of cell proliferation

4T1 cells at a density of 5×10³ cells/well in 96-well plates were incubated with varying drug formulations at different concentrations in pH 7.4 and pH 6.5 media. Following 3 h of treatment, the medium was removed and replaced by fresh medium. Then, the cells were irradiated with NIR laser (808 nm, 3 W/cm², 5 min) and incubated for another 45 h. Afterwards, the cell viability was evaluated by MTT assay.

In addition, LIVE/DEAD cell viability assay was also performed to visually observe the *in vitro*

chemo-photothermal therapy effect. Briefly, 4T1 cells at a density of 5×10^3 cells/well in 96-well plates were incubated with different drug formulations at equivalent doses of IR780 and DOX for 3 h. Then, the medium was replaced by fresh medium and the cells were exposed to 808 nm laser irradiation at 3 W/cm^2 for 5 min, followed by further culture for 21 h. Subsequently, the cells were stained with the LIVE/DEAD assay kit, and observed under a fluorescence microscope.

Cell apoptosis analysis

For cell apoptosis analysis, 4T1 cells were incubated with different drug formulations. Following 3 h of co-incubation, the medium was replaced by fresh medium. Then the cells were either treated with NIR laser as described above or left as controls, followed by another 21 h incubation. Subsequently, the apoptotic cells were stained using FITC-Annexin V Apoptosis Detection Kit I (KeyGen Biotech) and quantified using FACSCallibur (Becton Dickinson, San Jose).

Inhibition of cell migration

The inhibitory effects of mPEG-PAAV micelles/IR780+DOX with or without 808 nm laser irradiation on cell migration were measured in 4T1 cells using a transwell assay and a wound-healing assay. For the transwell assay, 4T1 cells were seeded in serum-free medium in the upper chamber, which also contained the different drug formulations at pH 6.5 or pH 7.4. Following 3 h of incubation, the medium in the upper chamber was replaced with fresh medium without FBS and the cells were either treated with laser (808 nm, 3 W/cm^2 , 5 min), or left as controls. After culturing for another 21 h, the non-migrated cells in the upper chamber were removed, and the migrated cells were stained with 0.1% crystal violet and photographed using an inverted microscope. The migrated cells were then de-stained in 30% acetic acid aqueous solution, and the OD value of the de-staining fluid at 540 nm was measured by a microplate reader (Tecan M200) to quantitatively estimate the migration rate [2].

For the wound-healing assay, 4T1 cells at a density of 2×10^5 cells/well were cultured in 6-well plates, and a sterile pipette was used to create the scratch. After treatment with free IR780+DOX or mPEG-PAAV micelles/IR780+DOX at pH 6.5 and pH 7.4 for 3 h, the medium was replaced by fresh medium and the cells were either treated with NIR laser as described above or left as controls. The migration distance was observed after 21 h of incubation using an inverted microscope [2].

Cellular uptake

Confocal laser scanning microscopy (CLSM) was employed to estimate the cell uptake capacity and intracellular release behaviour of mPEG-PAAV micelles/IR780+DOX in 4T1 cells. 4T1 cells cultured on a confocal imaging dish were treated with free IR780+DOX or mPEG-PAAV micelles/IR780+DOX at pH 6.5 and pH 7.4 for 3 h. Then, the medium was replaced by fresh medium and the cells were either treated with NIR laser as described above or left as controls. After another 3 h incubation, Hoechst 33342 was employed to stain the cell nuclei and the intracellular release of DOX was observed and photographed by CLSM (ZEISS LSM700).

In vitro PA imaging

For *in vitro* PA imaging, free IR780+DOX and mPEG-PAAV micelles/IR780+DOX at different concentrations were added into 0.5 mL tubes and then imaged with a photoacoustic imaging system (Endra Nexus128, USA) at a wavelength of 720 nm.

Bio-distribution of mPEG-PAAV micelles/IR780+DOX in tumor-bearing mice

When the subcutaneous 4T1 tumors grew up to 200-300 mm³, the mice were intravenously administered with mPEG-PAAV micelles/IR780+DOX and free IR780+DOX at the IR780 dose of 0.3 mg per kg mouse. *In vivo* NIR fluorescence images of the mice at pre-determined time intervals (2, 4, 8 and 24 h) were collected using an IVIS (Lumina XR Series III, PerkinElmer). Then, the organs and tumors from the above-treated tumor-bearing mice were collected at 24 h post-administration for *ex vivo* imaging.

Additionally, to measure the *in vivo* photoacoustic signal at the tumor site after intravenous administration of 0.9% NaCl, free IR780+DOX and mPEG-PAAV micelles/IR780+DOX for 24 h, the photoacoustic imaging system (Endra Nexus128, USA) with the laser at a wavelength of 720 nm and 7 ns pulse width was used. The photoacoustic signals at the focal depth of 5 mm in the tumor site were collected by 128 individual and unfocused transducers with the centre frequency of 5 MHz.

In vivo photothermal efficiency

Free IR780+DOX and mPEG-PAAV micelles/IR780+DOX were intravenously administered to the tumor-bearing mice at 0.5 mg/kg of IR780 and 0.65 mg/kg DOX. 24 h after administration, tumor tissues were exposed to NIR laser (808 nm, 1 W/cm^2) for 5 min. During the irradiation, the temperature change of tumor tissue was recorded using an infrared thermal imaging camera (Fluke Ti27).

In vivo therapeutic efficacy

The *in vivo* chemo-photothermal synergistic therapy efficiency of mPEG-PAAV micelles/IR780+DOX was estimated in balb/c mice bearing subcutaneous 4T1 tumors. When the tumor volume grew to 100-150 mm³, the mice were randomly divided into 8 groups (n=10), and intravenously administrated 0.9% NaCl and varying drug formulations at same doses of IR780 (0.5 mg/kg) and DOX (0.65 mg/kg) on day 0, 3 and 6; at 24 h post-injection, the tumor tissue in the experimental group was irradiated with 808 nm laser (1 W/cm², 5 min). The tumor volume and body weight were measured every day during the experiment. On day 7 and 29, 5 mice of each group were sacrificed by cervical dislocation. Their tumors were then harvested, weighed, photographed, and stained using TUNEL assay and H&E.

Additionally, to assess the biosafety of the application of mPEG-PAAV micelles/IR780+DOX, balb/c mice received the same treatments as described above, and their major organs were harvested and stained using H&E on day 29. Blood samples were collected *via* retro-orbital bleed and centrifuged (1610 g for 20 min at 4 °C) to get the plasma. Then, routine blood examination and evaluation of levels of aspartate transaminase (AST), creatinine (CRE), alanine aminotransferase (ALT) and urea nitrogen (BUN) in plasma were performed.

Statistical analysis

All data are expressed as the mean values ± standard deviations from at least triplicate separate experiments, which were analyzed using Student's t-test. P* < 0.05 or P** < 0.01 were considered statistically significant or markedly statistically significant, respectively.

Results and Discussion

Synthesis of mPEG-PAAV copolymer

The PAAV copolymer was synthesized using radical polymerization of AAm, AN and VIm. The mPEG-COOH was then conjugated to the terminal amine group of PAAV copolymer (Figure 2A). The structure of the polymer was characterized by ¹H-NMR spectra. As shown in Figure 2B-C, the characteristic resonances of PAAV and mPEG-PAAV copolymer are as follows: ¹H NMR (400 MHz, d⁶-DMSO) δ (ppm): 6.90-7.70 (m, imidazole), 1.66-2.30 (m, -CH₂- in -VIm-, -AN- and -AAm-), 3.50 (-CH₂-CH₂-O-). Additionally, the molecular weights of the polymers and the molar ratios of acrylamide/acrylonitrile/1-vinylimidazole were measured using GPC (Waters) and elemental analyser

(Eurovector EA3000), respectively, which are shown in Table S1.

Characterization of blank mPEG-PAAV micelles

The novel mPEG-PAAV copolymer could spontaneously form micelles using a dialysis method. As depicted in Figure 2D-E, the mPEG-PAAV micelles were 174.5 nm in average diameter with a narrow size distribution (PDI: 0.15) and spherical shape. Additionally, the size of the micelles did not show a remarkable change in a simulated physiological environment (PBS containing 10% FBS at pH 7.4), indicating that mPEG-PAAV micelles possessed good stability under the biological conditions (Figure 2F). Moreover, due to the protonation and deprotonation of PVIIm moiety at different pH [26], the zeta potentials of mPEG-PAAV micelles showed a substantial pH-dependence. As exhibited in Figure S1, the zeta potentials of mPEG-PAAV micelles approached neutral at physiological pH (7.4-7.0); however, they dramatically increased to 15.6-17.7 mV in the acidic environment when the pH value changed from 6.5 to 5.0.

Additionally, the biocompatibility of mPEG-PAAV micelles was also studied. As shown in Figure S2 and Figure S3, mPEG-PAAV micelles exhibited high hemocompatibility and negligible cytotoxicity, indicating that mPEG-PAAV micelle could be utilized as a safe drug carrier.

Temperature-sensitivity of mPEG-PAAV micelles

To demonstrate the formation and disruption of the micelles induced by temperature changes, temperature-dependent ¹H NMR spectra of the micelles were measured by observing the methylene peak of mPEG-PAAV backbone in D₂O (Figure 2G). With the increase of test temperature (25-65 °C), the relative peak area of methylene gradually increased, indicating that the core of mPEG-PAAV micelles was exposed to aqueous environment and hydrated in D₂O. Moreover, the size of the micelles increased as the temperature increased from 25 °C to 65 °C (Figure S4). Especially, when the temperature reached 65 °C, the mPEG-PAAV micelles disassembled and formed larger aggregates with diameters above 1 μm. We speculated that these results were caused by the transition of mPEG-PAAV copolymer from amphiphile to hydrophile during the heating process, which made the mPEG-PAAV micelles swell at temperatures above the UCST.

After ensuring the mPEG-PAAV micelles possessed thermal responsiveness, the UCST of mPEG-PAAV micelles was determined using

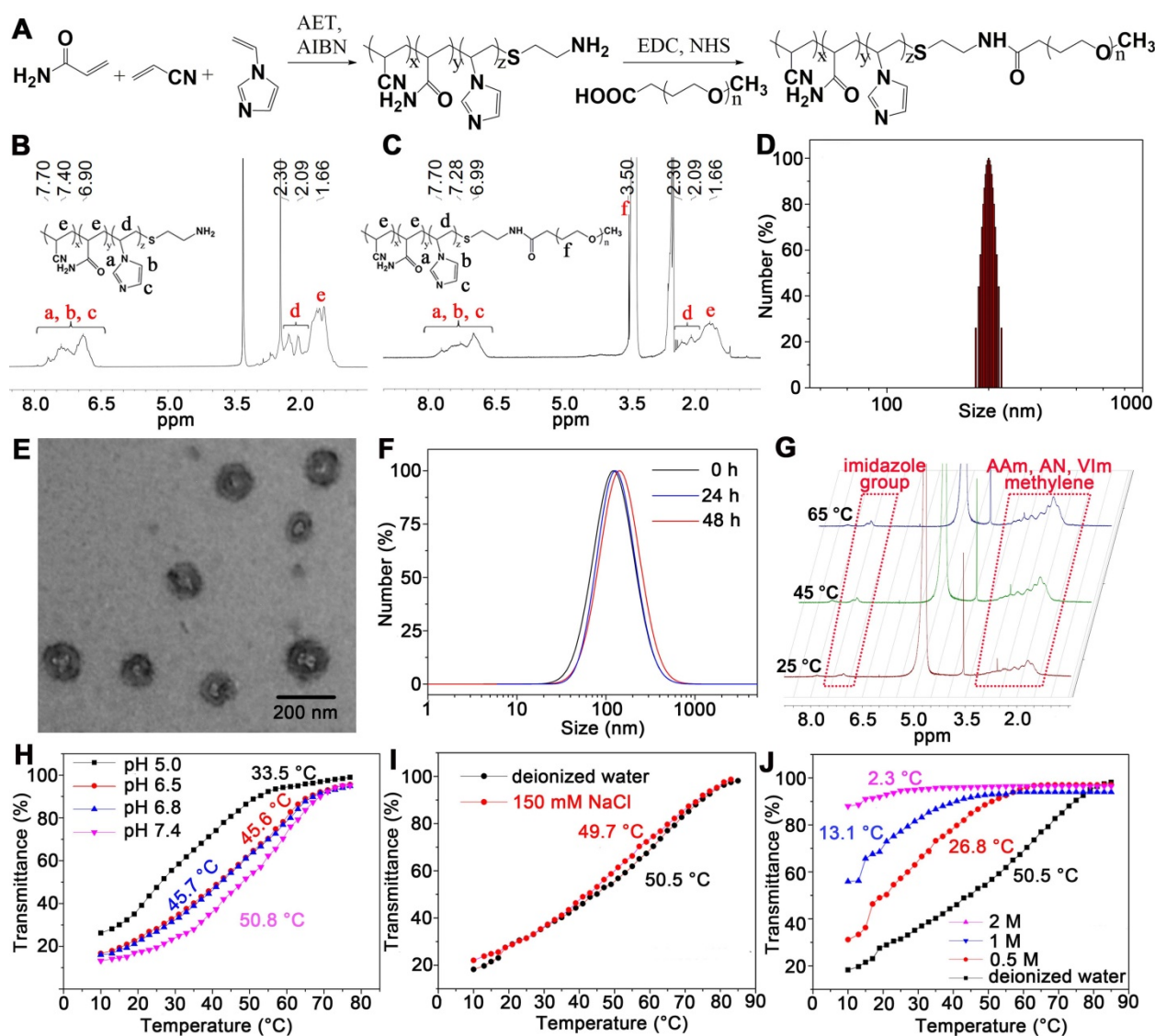


Figure 2. (A) Synthetic route of mPEG-PAAV copolymer. (B-C) $^1\text{H-NMR}$ spectra of PAAV copolymer and mPEG-PAAV copolymer, respectively. (D) Size distribution of mPEG-PAAV micelles. (E) TEM image of mPEG-PAAV micelles. (F) Size distribution of blank mPEG-PAAV micelles after incubation in PBS (pH=7.4) with 10% FBS at different intervals. (G) Variable temperature $^1\text{H-NMR}$ spectra of mPEG-PAAV micelles in D_2O solution. (H) Turbidity heating profiles of mPEG-PAAV micelle aqueous solutions (0.5 mg/mL) at varying pH values of pH 7.4, 6.8, 6.5 and 5.0, (I) at varying NaCl concentrations of 0 and 150 mM and (J) at varying urea concentrations of 0, 0.5, 1 and 2 M.

turbidity measurements. The aqueous solution of mPEG-PAAV micelles was opaque at low temperature while it became transparent at higher temperature, indicating that elevated temperature is a necessary parameter to break the intermolecular and intramolecular interactions (Figure S5). As shown in Figure 2H, the change of pH values also affected the micelles' UCST, which exhibited an obvious decline when the pH value was decreased. For example, compared to the UCST of mPEG-PAAV micelles at pH 7.4 (50.8 °C), it significantly decreased to 45.7 °C, 45.6 °C and 33.7 °C at pH 6.8, 6.5 and 5.0, respectively. We believe that this phenomenon is attributable to protonation of the imidazole group in the -VIm fragment. Because the hydrophobic effect plays a leading role in thermo-responsive behaviour [19], protonation of the imidazole group would increase

the hydrophilicity of the copolymer, decreasing the UCST of mPEG-PAAV micelles and facilitating the swelling or dissociation of the micelles. Additionally, Figure 2I shows that the UCST of mPEG-PAAV micelles is not significantly affected by electrolytes, which makes the micelles more suitable for the applications in biomedicine. However, when urea at different concentrations was added to the mPEG-PAAV micelles solution, there was an obvious decrease in the micelles' UCST (Figure 2J), indicating that their UCST was driven by intramolecular hydrogen bonding [27, 28].

In vitro photothermal efficiency

The basic characterizations (such as size, zeta-potential, drug loading efficacy and encapsulation efficiency) of drug-loaded micelles were first

measured. As summarized in **Table 1**, the average size of IR780- or DOX-loaded mPEG-PAAV micelles ranged from 180 nm to 240 nm. Moreover, their surface charges were close to neutral.

Table 1. Characterization of blank and IR780 or DOX-loaded mPEG-PAAV micelles (n=3).

Sample	Size (nm)	PDI	Zeta Potential (mV)	Loading (µg/mg)		Entrapment Efficiency (%)	
				DOX	IR780	DOX	IR780
Blank mPEG-PAAV micelles	174.5 ± 0.15 ± 6.7	0.15 ± 0.05	0.92 ± 0.2	/	/	/	/
mPEG-PAAV micelles/DOX	189.5 ± 0.32 ± 9.7	0.32 ± 0.01	6.45 ± 0.5	9.8 ± 3.3	/	70.6 ± 1.7	/
mPEG-PAAV micelles/IR780	234.2 ± 0.11 ± 11.8	0.11 ± 0.10	6.07 ± 0.3	/	8.1 ± 1.2	/	17.3 ± 7.3
mPEG-PAAV micelles/IR780+DOX	198.5 ± 0.25 ± 10.7	0.25 ± 0.10	3.82 ± 0.3	10.9 ± 2.4	8.4 ± 2.0	65.5 ± 4.5	19.7 ± 1.2

To confirm DOX and IR780 were loaded in mPEG-PAAV/micelles, the FTIR and XRD spectra of mPEG-PAAV micelles/IR780+DOX were measured. In **Figure S6**, all the characteristic peaks of blank mPEG-PAAV micelles appeared in FTIR spectra of drug-loaded mPEG-PAAV micelles. Moreover, three new peaks appeared (1512 cm⁻¹, 1231 cm⁻¹, 1164 cm⁻¹) in the spectrum of mPEG-PAAV micelles/IR780+DOX, which also appeared in the spectra of free DOX and free IR780. Additionally, the characteristic peaks of DOX and IR780 did not present in the XRD spectrum of mPEG-PAAV micelles/IR780+DOX as shown in **Figure S7**, indicating that DOX and IR780 were successfully encapsulated in mPEG-PAAV micelles in their amorphous form. Previous studies have demonstrated that when drugs are encapsulated into the particle in their amorphous form, they lose their crystallinity [29, 30].

The drug loading capacity of mPEG-PAAV micelles was quantified using fluorescence spectrometry (Hitachi F7000) at excitation wavelengths of 480 nm and 740 nm for DOX and IR780, respectively. Drug loadings of mPEG-PAAV micelle/IR780+DOX were 8.4 µg IR780 per mg of micelle and 10.9 µg DOX per mg of micelle; their encapsulation efficiencies were 19.7% (IR780) and 65.5% (DOX).

Then, we investigated the photothermal behaviour of mPEG-PAAV micelles/IR780+DOX in PBS under continuous laser (808 nm, 3 W/cm²) irradiation. After 400 s of irradiation, the temperature of mPEG-PAAV micelles/IR780+DOX solution increased by 20 °C, while there was only a 9 °C increase in the PBS group (**Figure 3A**). Moreover, the results in **Figure 3A** also showed that the significant temperature elevation was caused by IR780 but not DOX or mPEG-PAAV micelles. Additionally, the temperature increase of mPEG-PAAV micelles/IR780+DOX solution could be controlled by varying the concentration of IR780 and the laser power

density, which is shown in **Figure S8A-B**.

Next, each sample was irradiated with NIR laser for three cycles to further estimate the photothermal effect (**Figure 3B**). Due to their high photothermal efficiency, the mPEG-PAAV micelles/IR780+DOX solution exhibited a greater increase in temperature than free IR780+DOX after the same irradiation time in the first cycle. However, we believe that some IR780 were released from the micelles after laser irradiation. Moreover, the IR780 could transfer energy from NIR laser irradiation to the oxygen nearby and generate singlet oxygen (**Figure S9**), which would degrade IR780 into several carbonyl compounds [31, 32]. Thus, the hyperthermia induced by both mPEG-PAAV micelles/IR780+DOX and free IR780+DOX decreased in the second and third cycles. In contrast, the free IR780+DOX group showed a more severe decrease and exhibited no differences compared with PBS, suggesting rapid degradation of free IR780. However, due to the fluorescence quenching of IR780 in the micelle (the fluorescence quenching efficiency is 36.03%) (**Figure S10**) and the photostability protection of mPEG-PAAV micelle, the IR780 encapsulated in mPEG-PAAV micelles degraded more slowly and still produced a notable hyperthermia effect, which implied that the photothermal properties of IR780 in mPEG-PAAV micelles were significantly improved. To further demonstrate the photostability protection of mPEG-PAAV micelles, we also measured the photobleaching efficiency of IR780 in free IR780+DOX and mPEG-PAAV micelle/IR780+DOX group after NIR laser irradiation for 3 cycles. As shown in **Figure S11**, 33.4% of fluorescence was bleached in free IR780+DOX group after first cycle of laser irradiation, however, the photobleaching efficiency was only 9.4% in mPEG-PAAV micelle/IR780+DOX. Additionally, compared to mPEG-PAAV micelle/IR780+DOX, more fluorescence signals were bleached by laser irradiation in free IR780+DOX group after 3 cycles of laser irradiation, indicating that mPEG-PAAV micelle possessed a better capacity of protecting the photostability of IR780.

Drug release properties of mPEG-PAAV micelles/IR780+DOX

In order to estimate the pH- and thermo-sensitive drug release capacity, mPEG-PAAV micelles/IR780+DOX solution was heated in a thermostatically controlled bath at different pH values. As depicted in **Figure 3C**, the cumulative release percentage of DOX from mPEG-PAAV micelles in pH 7.4 at 45 °C was obviously higher than that at body temperature (37 °C) and room temperature (25 °C). Additionally, as demonstrated

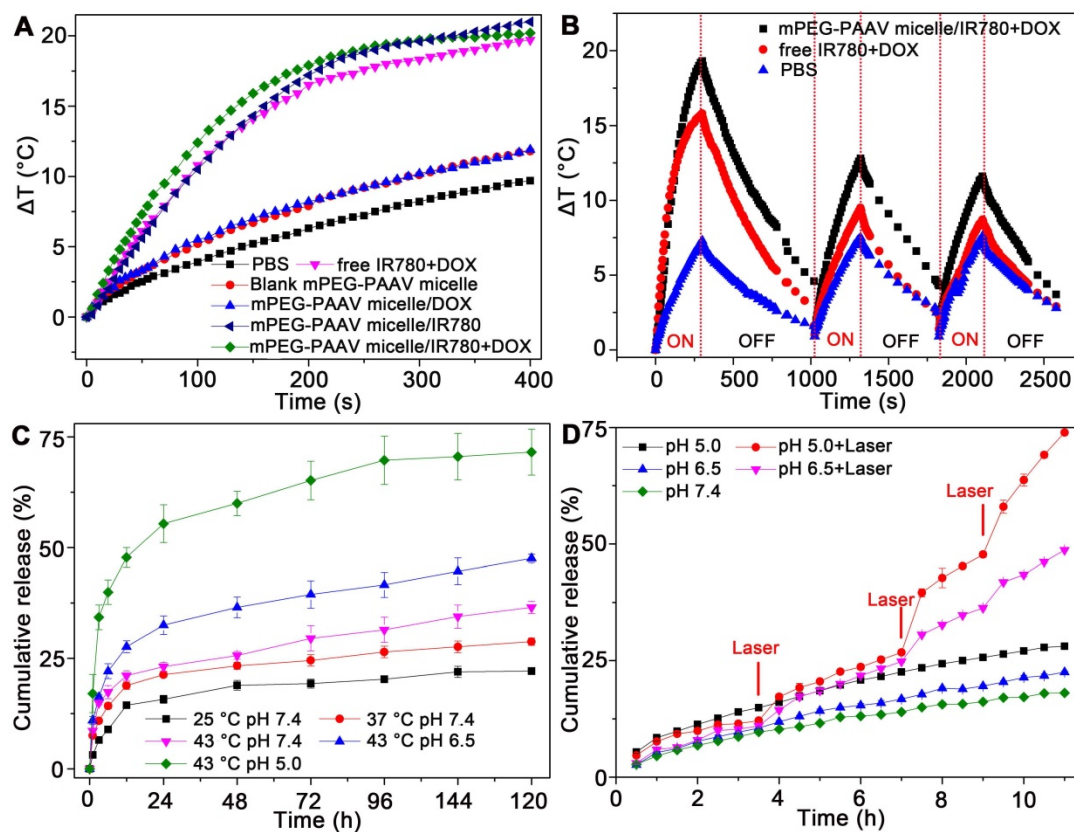


Figure 3. (A) The temperature changes of PBS, free IR780+DOX, blank and drug-loaded mPEG-PAAV micelles under NIR laser irradiation (808 nm, 3 W/cm²). (B) Photothermal stability of mPEG-PAAV micelles/IR780+DOX under 808 nm laser irradiation (3 W/cm²) for 3 cycles. (C) The cumulative release of DOX from mPEG-PAAV micelles in different pH solution (pH 7.4, 6.5 and 5.0) at 25 °C, 37 °C and 45 °C. (D) The effects of laser irradiation (808 nm, 3 W/cm², 5 min for each time) on the DOX release rate (n=3).

above, the UCST of mPEG-PAAV micelles was close to or below 45 °C in acidic conditions such as the lysosomal environment (pH 5.0) and the tumor extracellular environment (pH 6.5). Therefore, the DOX release from mPEG-PAAV micelles/IR780+DOX at pH 6.5 and pH 5.0 at 45 °C was significantly accelerated in comparison to that at pH 7.4. For example, the mPEG-PAAV micelles/IR780+DOX in pH 6.5 and pH 5.0 at 45 °C released up to 32.5% and 55.3% of DOX within 24 h, respectively; around 47.5% and 71.5% of DOX was released at the end of the incubation period, respectively. In contrast, by 144 h, only 36% of DOX was released from mPEG-PAAV micelles/IR780+DOX incubated in pH 7.4 at 45 °C. Thus, these results show that the DOX release rate is accelerated with the increase of temperature and decrement of pH value, suggesting that the mPEG-PAAV micelles possess pH- and thermo-sensitive drug release capacity.

Next, the NIR laser-induced drug release efficiency was measured, as shown in Figure 3D. Although the DOX release from mPEG-PAAV micelles was accelerated with the decrease of pH value, the cumulative drug release at pH 7.4, 6.5 and 5.0 were all less than 25% after 11 h of incubation without laser irradiation, indicating there was

minimal undesirable drug leakage. Conversely, due to hyperthermia (above the UCST) induced by IR780 under NIR laser irradiation, the micellar structure of mPEG-PAAV micelle was destroyed. As a result, the DOX release percentage at pH 5.0 and 6.5 after laser irradiation (808 nm, 3 W/cm², 5 min) for 3 times were 2.6-fold and 2-fold higher than those without laser irradiation, respectively. More importantly, the drug release of mPEG-PAAV micelles/IR780+DOX can be directly controlled by laser irradiation, which will help to improve the drug distribution and avoid drug leakage during systemic circulation.

Cellular uptake and intracellular distribution

The cellular uptake efficiency of mPEG-PAAV micelles in 4T1 cells was investigated using CLSM. As demonstrated above, the surface charge of mPEG-PAAV micelles could become positively charged in weakly acidic environments (pH 6.5-5.0). Thus, in comparison to the treatment at pH 7.4, there was an enhanced red fluorescent signal in 4T1 cells after the treatment with mPEG-PAAV micelles/IR780+DOX at pH 6.5 (Figure S12). However, a large amount of red fluorescence remained in the state of aggregation at pH 6.5, indicating an incomplete release of DOX from mPEG-PAAV micelles. In

contrast, after the treatment of mPEG-PAAV micelles/IR780+DOX under NIR laser irradiation (808 nm, 3 W/cm², 5 min) at pH 6.5, there was a significant elevation of red fluorescence intensity throughout the 4T1 cells. This phenomenon was caused by the increased permeability and fluidity of the plasma membrane due to IR780-induced hyperthermia, which augmented the retention of mPEG-PAAV micelles/IR780+DOX inside the 4T1 cells. More importantly, due to the hyperthermia induced by IR780 under NIR laser irradiation, the mPEG-PAAV micelles would swell and dissociate in lysosomes, facilitating the intracellular DOX release from mPEG-PAAV micelles. Thus, red fluorescence evenly distributed throughout the 4T1 cells. Based on the above results, it is demonstrated that the hyperthermia caused by NIR laser irradiation is able to enhance the cellular uptake efficiency of the mPEG-PAAV micelles/IR780+DOX and accelerate the intracellular drug release from micelles.

In vitro chemo-photothermal therapy

To estimate *in vitro* chemo-photothermal therapy efficacy of mPEG-PAAV micelles/IR780+DOX, the viability of 4T1 cells was measured by MTT assay. After treatment with varying drug formulations at pH 7.4 or 6.5 for 3 h, the medium was removed and the cells were irradiated with NIR laser or left as controls, followed by further incubation for 45 h. **Figure 4A-C** shows that the cell viability decreases with increasing DOX concentration, either in the form of free drug or drug-loaded micelles. However, there was no obvious cell growth inhibition induced by IR780 without NIR laser irradiation. Additionally, the cell viability of 4T1 cells treated with mPEG-PAAV micelles/IR780+DOX at pH 6.5 was not significantly enhanced in comparison to that at pH 7.4, even though the cellular uptake of mPEG-PAAV micelle at pH 6.5 was higher than that at pH 7.4. In contrast, when the treatment of mPEG-PAAV micelles/IR780+DOX at pH 6.5 was combined with NIR laser irradiation, the hyperthermia induced by mPEG-PAAV micelles/IR780+DOX would not only damage breast cancer cells and boost the DOX release, but also significantly enhance the cytotoxicity of DOX to facilitate the synergistic chemo-photothermal therapy effect [8-10]. Although a similar effect also appeared in the free IR780+DOX group irradiated with NIR laser (especially at higher concentration), its synergistic effect was not comparable to mPEG-PAAV micelles/IR780+DOX. To explain this phenomenon, we also measured the media temperature of free IR780+DOX and mPEG-PAAV micelles/IR780+DOX at pH 6.5 after 5 min of irradiation. We found that the increase of temperature in the free IR780+DOX group was lower

than that in the mPEG-PAAV micelles/IR780+DOX group, which was consistent with the results of the *in vitro* photothermal effect studies. For example, the media temperatures in the free IR780+DOX group and mPEG-PAAV micelles/IR780+DOX group (DOX: 0.4 µg/mL, IR780: 0.3 µg/mL) reached 41.1 °C and 44.6 °C after 5 min laser irradiation, respectively. Thus, the treatment of mPEG-PAAV micelles/IR780+DOX at pH 6.5 with NIR laser irradiation induced the strongest cytotoxicity compared to other treatments.

Table 2. IC₅₀ values (DOX µg/mL) of free IR780+DOX and mPEG-PAAV micelles/IR780+DOX (n=5).

Sample	IC ₅₀ of DOX (µg/mL)		
	pH 7.4	pH 6.5	pH 6.5 + Laser
Free IR780+DOX	0.18	0.16	0.11
mPEG-PAAV micelles/IR780+DOX	0.37	0.25	0.05

The IC₅₀ values of free IR780+DOX and mPEG-PAAV micelles/IR780+DOX were also calculated. As shown in **Table 2**, the IC₅₀ value (DOX) of mPEG-PAAV micelles/IR780+DOX (0.05 µg/mL) was remarkably lower than that of the other drug formulations, suggesting that the cytotoxic effect of mPEG-PAAV micelles/IR780+DOX on 4T1 cells could be improved by NIR laser irradiation. To estimate whether there was a synergy between PTT and chemotherapy, the therapeutic efficiency was measured by subtracting the percentage of viable cells from 100%. And the following equation was employed to calculate the additive therapeutic efficacy of each group: $E_{\text{additive}} = 100\% - (f_{\text{photothermal}} \times f_{\text{chemo}}) \times 100\%$, where *f* was the percentage of viable cells after the treatment with mPEG-PAAV micelles/IR780+DOX and free IR780+DOX [9, 33]. The results in **Table S2** showed that the measured therapeutic efficiency of chemo-photothermal therapy in the group of mPEG-PAAV micelles/IR780+DOX plus laser irradiation was enhanced in comparison to the additive therapeutic efficiency of chemotherapy and photothermal therapy (especially at higher concentration), suggesting that the mPEG-PAAV micelles/IR780+DOX combined with NIR laser irradiation could achieve a synergistic effect for killing the breast cancer cells. Additionally, the combination index (CI) of mPEG-PAAV micelles/IR780+DOX at pH 6.5 plus NIR irradiation was also calculated using the following formula: $CI = C_1 / C_d + C_2 / C_i$, where *C*₁ and *C*₂ are the IC₅₀ values of DOX (0.05 µg/mL) and IR780 (0.042 µg/mL) in mPEG-PAAV micelles/IR780+DOX at pH 6.5 with NIR irradiation, respectively. *C*_d and *C*_i are the IC₅₀ values of DOX (0.31 µg/mL) in mPEG-PAAV micelles/DOX and IR780 (0.088 µg/mL) in

mPEG-PAAV micelles/IR780 at pH 6.5 with NIR irradiation, respectively. It is reported that a CI value lower than 1 indicates synergy [2, 16]. According to the above calculation, the CI value of mPEG-PAAV micelles/IR780+DOX at pH 6.5 with NIR laser irradiation is 0.65, which further confirms their chemo-photothermal synergetic therapeutic effect.

To visually estimate the combinational therapy efficiency, the 4T1 cells in the presence of free IR780+DOX and mPEG-PAAV micelles/IR780+DOX were irradiated with NIR laser or left as controls. The

dead and live cells were stained by PI and calcein-AM in red and green colors, respectively. **Figure 4D** shows that there is almost no cell necrosis in the group that received NIR laser irradiation alone, implying that laser irradiation at 3 W/cm² is relatively safe for *in vitro* therapy. In addition, laser irradiation of cells treated with mPEG-PAAV micelles/IR780+DOX at pH 6.5 resulted in an increase of red fluorescence in 4T1 cells, indicating more cells were killed after chemo-photothermal therapy using mPEG-PAAV micelles.

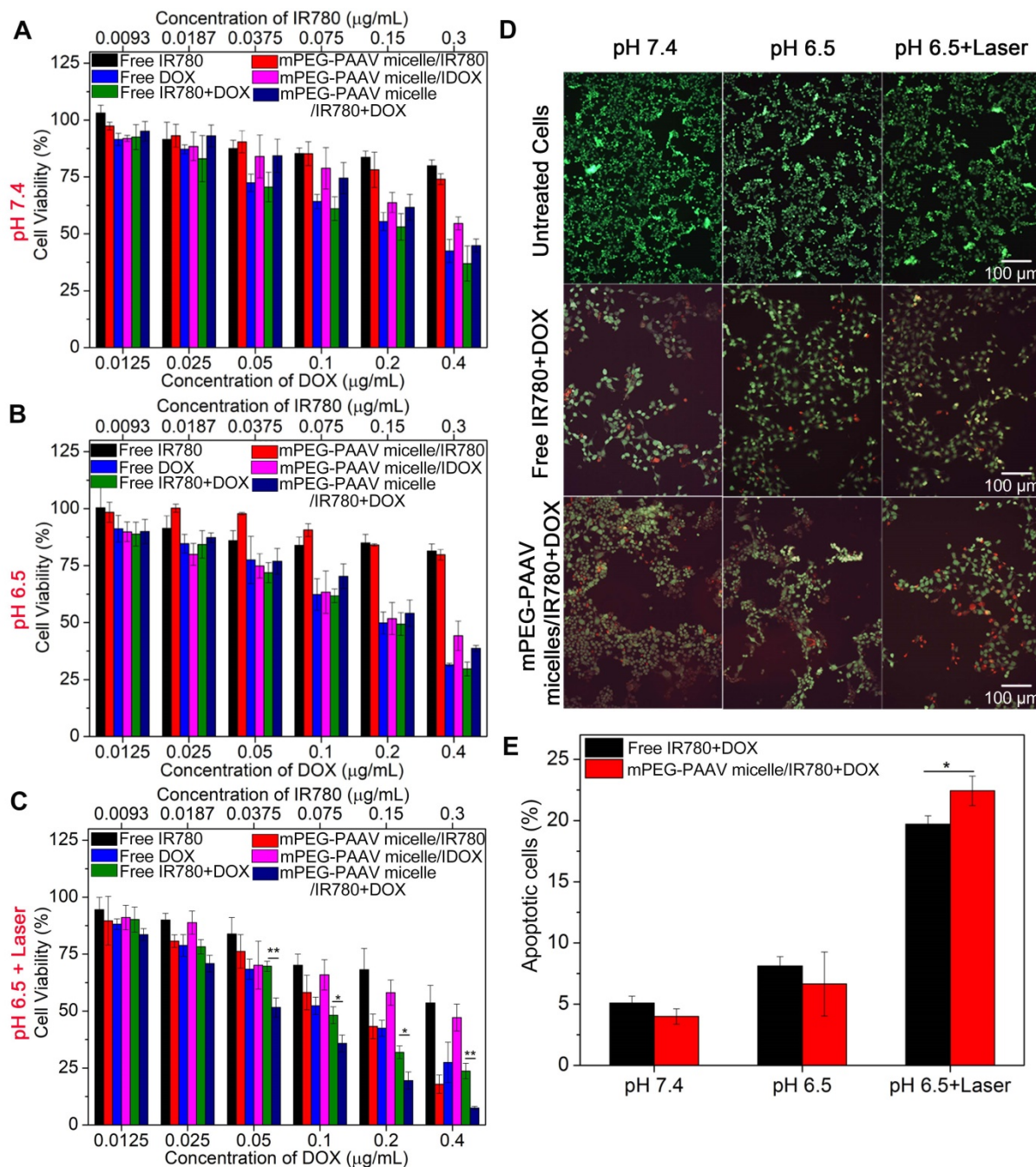


Figure 4. (A-C) The viability of 4T1 cells incubated with varying drug formulations at pH 7.4 and 6.5 with or without laser irradiation at wavelength of 808 nm (3 W/cm², 5 min) (n=5). (D) Fluorescence images of calcein-AM/PI stained 4T1 cells and (E) percentage of apoptotic 4T1 cells after treatment with free IR780+DOX and mPEG-PAAV micelles/IR780+DOX at pH 6.5 and 7.4 with or without laser irradiation at 808 nm (3 W/cm², 5 min) (n=3).

Additionally, the hyperthermia-assisted chemotherapy also showed a positive effect on inducing cancer cell apoptosis. **Figure 4E** exhibits that the treatments of both free IR780+DOX and mPEG-PAAV micelles/IR780+DOX under NIR laser irradiation significantly induced cell apoptosis. Especially, the cell apoptosis percentage reached 22.4% for the mPEG-PAAV micelles/IR780+DOX at pH 6.5 with NIR laser irradiation group, which was 1.2-fold higher than that of the free DOX+IR780 at pH 6.5 with NIR laser irradiation group as well as 5.6- and 3.4-fold higher than those at pH 7.4 and 6.5 without NIR laser irradiation, respectively.

Therefore, we conclude that due to the surface charge reversion of mPEG-PAAV micelles and the enhanced permeability and fluidity of the plasma membrane by laser-induced hyperthermia, more therapeutic agents encapsulated in mPEG-PAAV micelles could be delivered into the cancer cells, which is crucial for achieving sufficient therapeutic effect [8, 9]. Moreover, because of the protonation of imidazole groups of mPEG-PAAV copolymer in acidic condition, the increased hydrophilicity of the polymer would lead to a decrease in the polymer's UCST (especially at pH 5.0), resulting in a sufficient

intracellular drug release under NIR laser irradiation. More importantly, cancer cells are more sensitive to chemotherapeutics under hyperthermia and the direct cytotoxicity of temperatures >43 °C can contribute to the synergistic effect [34-36]. Accordingly, the direct hyperthermia therapeutic effects cannot be separated from increased drug uptake/release and drug sensitivity using this micellar system, and the mPEG-PAAV micelles/IR780+DOX under NIR laser irradiation achieved a synergistic therapy effect *in vitro*.

Inhibition of 4T1 cell migration

Because lung metastasis of breast cancer is the major cause of failure after surgery, radiation or chemotherapy [37, 38], the inhibitory effect of mPEG-PAAV micelles/IR780+DOX on breast cancer cell migration is required to estimate the efficiency of chemo-photothermal therapy. The migration capacity of 4T1 cells after chemo-photothermal therapy was measured using a wound-healing assay and a transwell assay. **Figure 5A-B** show the wound-healing response of 4T1 cells after treatment with varying drug formulations with or without NIR laser irradiation. For untreated 4T1 cells, they renewed

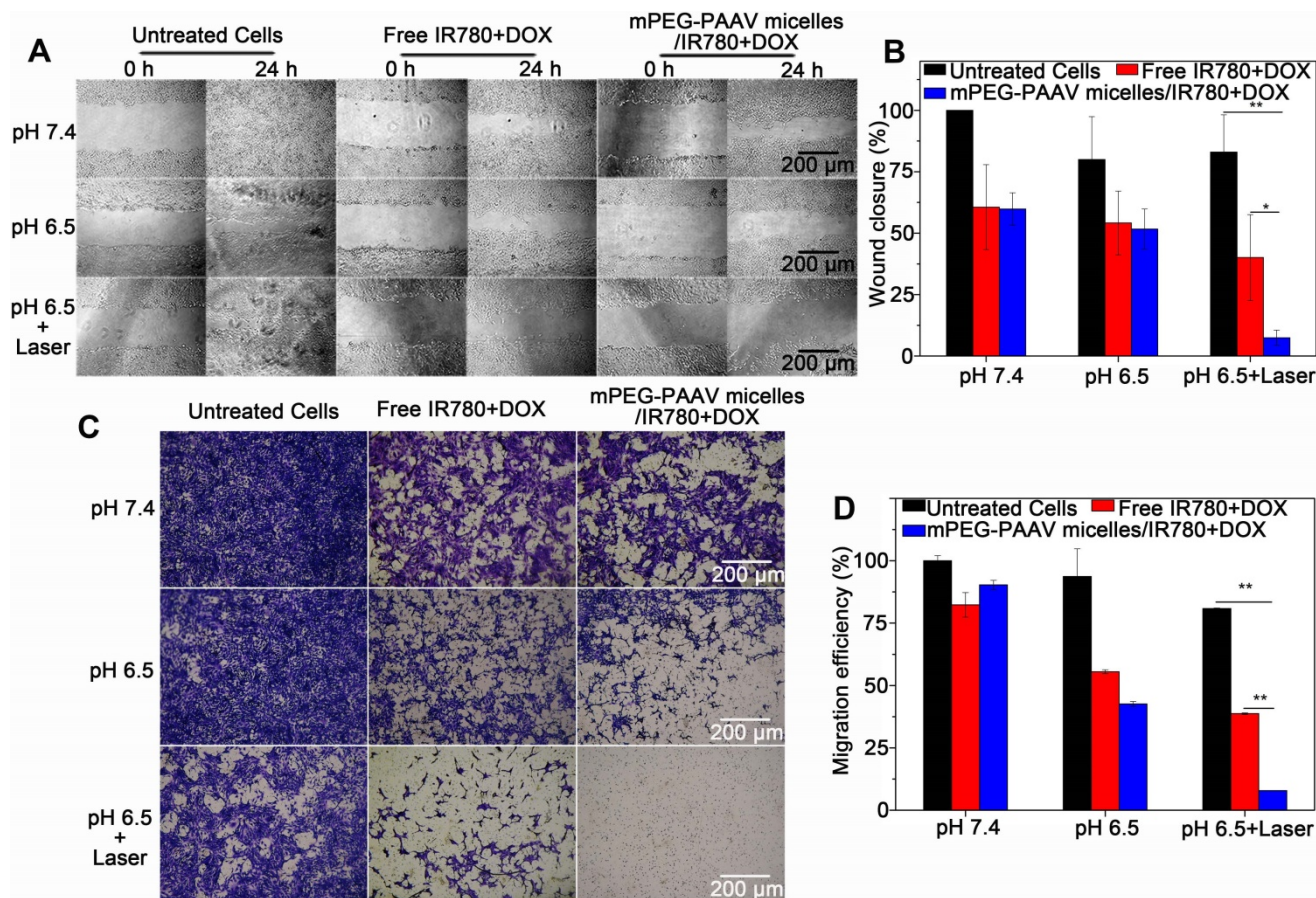


Figure 5. (A-B) The wound-healing response, and (C-D) transwell migration assay of 4T1 cells treated with varying drug formulations at pH 6.5 and 7.4 with or without 808 nm laser irradiation (3 W/cm², 5 min) (n=3).

rapidly and the scratch wound recovered quickly. Compared to the treatment with free IR780+DOX and mPEG-PAAV micelles/IR780+DOX at pH 7.4 and 6.5 without irradiation, the mPEG-PAAV micelles/IR780+DOX treatment plus NIR laser irradiation tended to suppress the scratch wound healing of 4T1 cells more effectively, resulting in a wound closure of only 7.4%. Additionally, in the transwell assay, the mPEG-PAAV micelles/IR780+DOX treatment plus NIR laser irradiation also presented the strongest capacity for inhibiting 4T1 cell migration (Figure 5C-D). These results demonstrated that the chemo-photothermal therapy using mPEG-PAAV micelles/IR780+DOX could effectively suppress the migration of breast cancer cells *in vitro*.

Bio-distribution of mPEG-PAAV micelles/IR780+DOX in tumor-bearing mice

Tumor-bearing balb/c mice were intravenously administrated free IR780+DOX and mPEG-PAAV micelles/IR780+DOX, and the IR780 circulation and bio-distribution were studied using an IVIS fluorescence imaging system. In the mPEG-PAAV micelles/IR780+DOX group, the IR780 fluorescence signal at the tumor site gradually increased and reached the maximum level at 24 h post-injection (Figure 6A). This result indicated that the mPEG-PAAV micelles/IR780+DOX were effectively targeted to the solid breast tumor by the enhanced permeability and retention (EPR) effect. By comparison, the tumor fluorescence intensity in the mice treated with free IR780+DOX was significantly

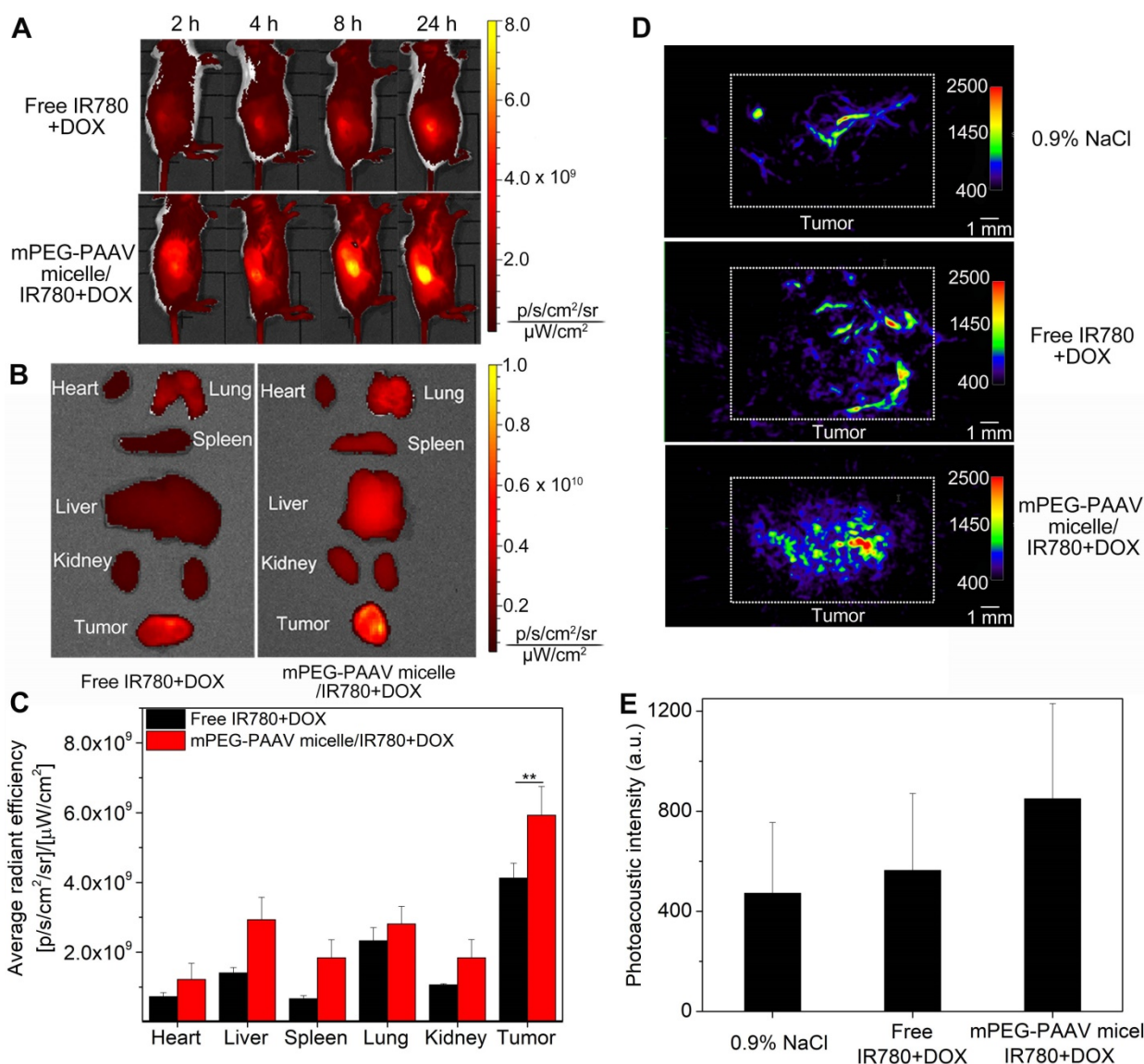


Figure 6. (A) NIR fluorescence imaging of balb/c mice bearing subcutaneous 4T1 tumors intravenously administrated with free IR780+DOX and mPEG-PAAV micelles/IR780+DOX at 2 h, 4 h, 8 h and 24 h. (B) Ex vivo NIR fluorescence imaging of the harvested organs and tumors at 24 h post-administration (n=4). (C) Quantitative analysis of IR780 fluorescence intensity in tumor. (D-E) Photoacoustic imaging of tumor 24 h after intravenous administration of varying drug formulations (n=4, the focal depth in the tumor site is 5 mm).

weaker due to their rapid clearance rate. To quantitatively estimate their bio-distribution, the major organs (heart, liver, spleen, lung and kidney) as well as tumors were collected for *ex vivo* imaging (Figure 6B-C). The fluorescence signal intensity of the tumor in the mPEG-PAAV micelles/IR780+DOX group was the strongest among all tissues, which was also 1.44-fold higher than that in the free IR780+DOX group. Thus, the mPEG-PAAV micelles possess a prolonged blood circulation and achieved a preferable passive targeting ability, which are the key factors for superior combination therapy.

In vitro and in vivo PA imaging of mPEG-PAAV micelles/IR780+DOX

IR780 can be used as an excellent PA imaging agent as well as a photothermal agent [25]. Herein, the *in vitro* PA imaging of free IR780+DOX and mPEG-PAAV micelles/IR780+DOX is shown in Figure S13, in which the PA intensity depends on the IR780 concentration. Such a significant PA contrast effect could be used to visualize the tumor morphology and microvascular distribution *in vivo*. As depicted in Figure 6D-E, when the mice were treated with 0.9% NaCl, only the microvasculature in the tumor could be visualized. However, after intravenous administration of mPEG-PAAV micelles/IR780+DOX and free IR780+DOX, the PA signal in the tumor tissue was enhanced obviously at 24 h post-injection. Especially in the mPEG-PAAV micelles/IR780+DOX group, the PA signals were 1.8-fold and 1.5-fold higher than those in the 0.9% NaCl and free IR780+DOX groups, respectively, which coincided with the *in vivo* NIR fluorescence imaging behavior. These results suggested that the mPEG-PAAV micelles/IR780+DOX-based PA imaging provided an effective approach to know the distribution of mPEG-PAAV micelles/IR780+DOX at the tumor site and obtain more information about the microstructure of the tumor.

In vivo photothermal efficiency

In order to estimate the *in vivo* photothermal conversion performance of mPEG-PAAV micelles/IR780+DOX plus NIR laser irradiation, a single dose of different drug formulations was intravenously administrated into mice bearing 4T1 tumors, and the tumors were exposed to the 808 nm NIR laser (1 W/cm², 5 min) at 24 h post-administration. Whole-body infrared thermal images were captured using an infrared camera during the NIR laser irradiation. The tumor temperature of the mice receiving the intravenous administration of mPEG-PAAV micelles/IR780+DOX rapidly increased by 20 °C, which was higher than that of the free IR780+DOX (9.6 °C) group

and the 0.9% NaCl group (8.0 °C) (Figure 7A-B). It has been demonstrated that hyperthermia over 50 °C can induce cancer cell necrosis [39]; moreover, when intra-tumor temperatures exceed 45 °C, DOX release is also enhanced due to the thermo- and pH-sensitivity of mPEG-PAAV micelles. Thus, we speculated that the chemo-photothermal synergistic therapy using mPEG-PAAV micelles/IR780+DOX could inhibit regrowth of the tumor to a large extent.

In vivo therapy efficiency

To estimate the *in vivo* chemo-photothermal synergistic therapy, mice bearing 4T1 tumors were treated with different drug formulations on day 0, 3 and 6; at 24 h post-injection, the tumor tissue was exposed to NIR laser at a wavelength of 808 nm (1 W/cm², 5 min). On day 7 post-injection, 5 mice from each group were randomly chosen and their tumor tissues were excised for histopathological examination. In comparison to the other groups, H&E staining of the tumor slices treated with mPEG-PAAV micelles/IR780+DOX plus NIR laser irradiation showed more severe damage, indicating more tumor necrosis was induced by this treatment (Figure 7C). These results agreed with the TUNEL staining assay, which further demonstrated the excellent chemo-photothermal therapeutic efficacy of mPEG-PAAV micelles/IR780+DOX (Figure 7D).

In order to further estimate the *in vivo* therapy efficacy of mPEG-PAAV micelles/IR780+DOX, we continued to measure the tumor growth profiles of the remaining mice from each group for 29 days after the treatment described above. As shown in Figure 7E, the tumors in the 0.9% NaCl group with or without laser irradiation grew normally, implying that the growth of tumor was not affected by NIR laser irradiation at the used power density (1 W/cm², 5 min). The free IR780+DOX treatment with or without NIR laser irradiation did not show an obvious inhibition on 4T1 tumor growth, which was caused by the lower accumulation of IR780 and DOX at the tumor site. Because of the preferable passive targeting ability of mPEG-PAAV micelles, more DOX and IR780 could be delivered to the tumor tissue and moderate tumor suppression was achieved by the treatment of mPEG-PAAV micelles/DOX, mPEG-PAAV micelles/IR780 with NIR laser irradiation and mPEG-PAAV micelles/IR780+DOX without NIR laser irradiation. However, tumor recurrence was observed in these treatment arms, and the tumor volume eventually increased 10-18 folds relative to the original volume, indicating that the chemotherapy or photothermal therapy alone were unable to completely eliminate the 4T1 tumor. By comparison, the mPEG-PAAV micelles/IR780+DOX plus NIR

laser irradiation remarkably inhibited tumor growth. Especially on day 9, the tumors in the mPEG-PAAV micelles/IR780+DOX plus NIR laser irradiation group disappeared and no recurrence was observed during the whole experimental period. Additionally, the results of tumor weight and morphology at the end of the experiment also presented a similar trend to the above findings (Figure 7F-G). To further estimate their antitumor capacity, tumor specimens were collected on 29th day post-administration, and

were prepared for H&E staining. As shown in Figure S14, there were no cancer cells observed in H&E-stained tissues of the group treated with mPEG-PAAV micelles/IR780+DOX plus NIR laser irradiation, suggesting that the tumor was completely eliminated. Therefore, these results demonstrated that the combination of mPEG-PAAV micelles/IR780+DOX treatment and NIR laser irradiation exhibited the best synergistic therapy effect on tumor elimination.

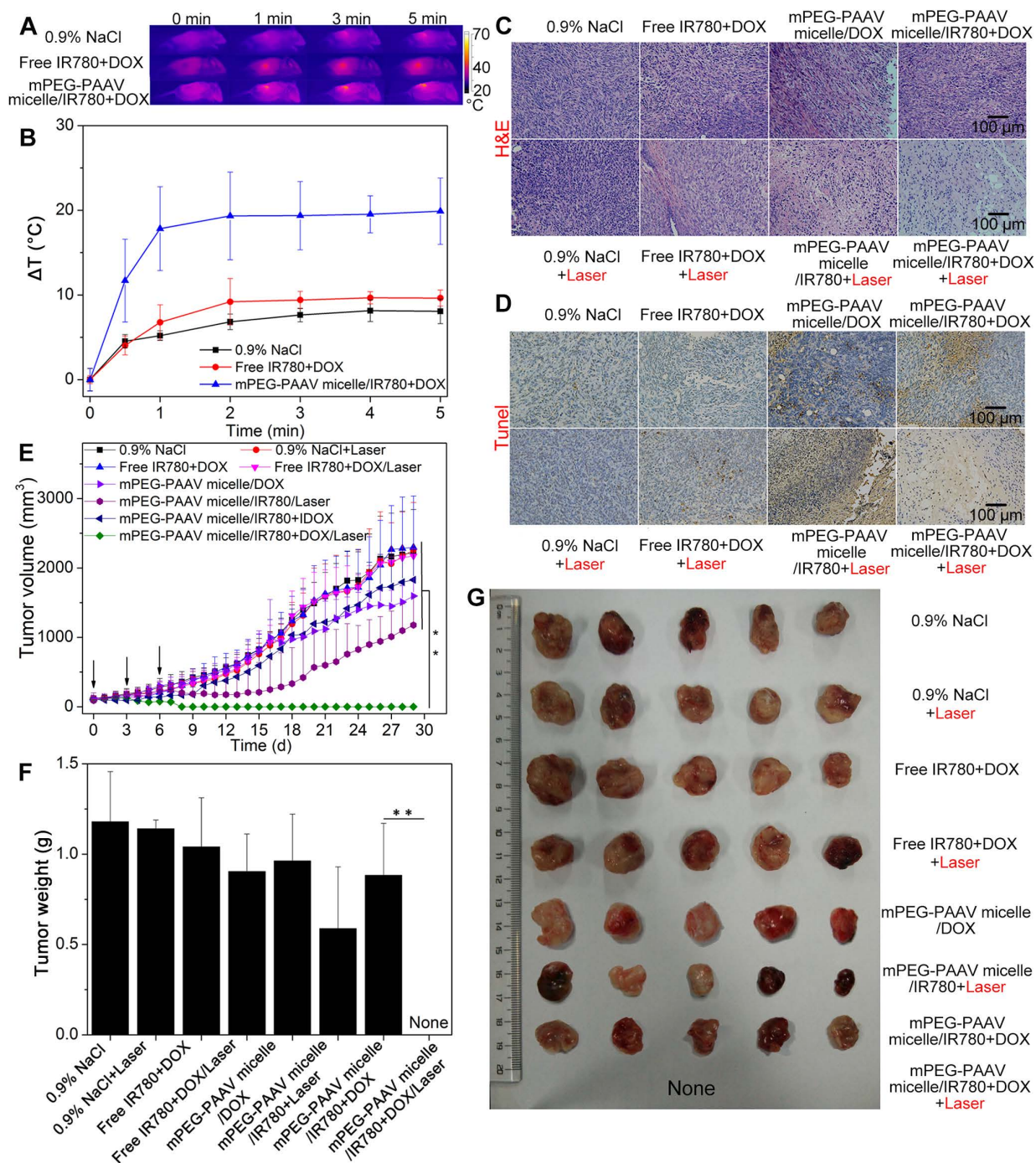


Figure 7. (A) Thermal imaging and (B) the temperature change at the tumor site of mice bearing 4T1 tumors treated with varying drug formulations via the tail-vein upon 808 nm laser irradiation (1 W/cm², 5 min) (n=4). (C) H&E and (D) TUNEL stained images of the tumors from mice treated with 0.9% NaCl, free IR780+DOX, mPEG-PAAV micelles/DOX, mPEG-PAAV micelles/IR780 and mPEG-PAAV micelles/IR780+DOX (i.v.) with or without laser exposure (1 W/cm², 5 min) on day 7 (n=5). (E) The tumor growth profiles from each group. (F) The weight and (G) morphology of tumors at the experimental end point (n=5).

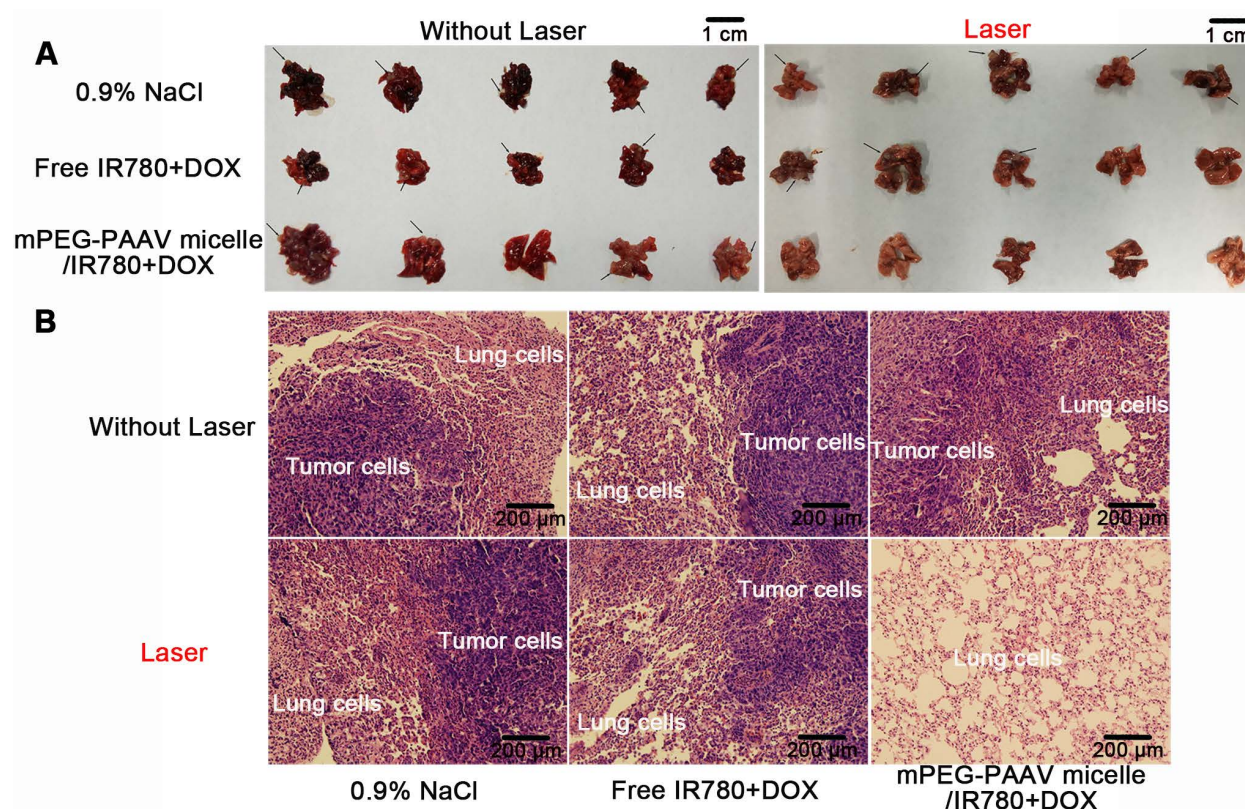


Figure 8. (A) Morphology and **(B)** H&E images of lungs from mice bearing 4T1 tumor injected with varying drug formulations with or without laser irradiation at a wavelength of 808 nm (1 W/cm², 5 min). Black arrows represented the foci of tumor metastases (n=5).

In vivo anti-lung metastasis of breast cancer

Lung metastasis is a common phenomenon at the later stage of breast cancer and is closely correlated with death in breast cancer [40]. Thus, in this study, all 5 mice in the 0.9% NaCl group with or without laser irradiation formed many lung metastases at the end of the *in vivo* treatment, with about 12 metastasized nodules formed in the lung (**Figure 8A and Table 3**). Although the treatment with free IR780+DOX with and without NIR laser irradiation and mPEG-PAAV micelles/IR780+DOX without NIR laser exposure suppressed the lung metastasis of 4T1 cells to some extent, the occurrence rate of lung metastases and the number of metastatic nodules still remained above 60% and 6, respectively. Fortunately, in addition to completely eliminating the subcutaneous 4T1 tumors, treatment with mPEG-PAAV micelles/IR780+DOX plus NIR laser irradiation could thoroughly suppress the lung metastasis of breast cancer cells. These results were further confirmed by H&E staining of lung tissues at the end of the *in vivo* treatment. In **Figure 8B**, the H&E-stained lung tissues of the group treated with mPEG-PAAV micelles/IR780+DOX plus NIR laser irradiation exhibited no detectable foci of tumor metastases. Thus, it was demonstrated that chemo-photothermal therapy using mPEG-PAAV micelles

can completely suppress lung metastasis of breast cancer cells.

Table 3. Occurrence rate of lung metastasis and number of metastatic nodules after different treatments (n=5).

Sample	Occurrence rate of lung metastasis (%)		Number of metastatic nodules	
	Without laser	With laser	Without laser	With laser
0.9% NaCl	100	100	11.8±4.3	12.5±3.7
Free IR780+DOX	80	60	8.2±3.9	5.7±1.5
mPEG-PAAV micelle/IR780+DOX	80	0	6.0±1.0	0

Based on the results discussed above, mPEG-PAAV micelles/IR780+DOX plus NIR laser irradiation showed a preferable chemo-photothermal synergistic therapy efficacy, which not only eliminated the subcutaneous 4T1 tumor, but also thoroughly inhibited the lung metastasis of breast cancer. We believe that this effective therapy effect is due to the following factors: (1) due to the thermo- and pH-sensitivity of mPEG-PAAV micelles, the drug release can be precisely controlled by NIR laser irradiation, improving the bioavailability of drugs and avoiding drug leakage during *in vivo* circulation; (2) the synergistic effect of the chemo-photothermal therapy can effectively inhibit breast cancer proliferation and metastasis. Therefore, all these advantages are beneficial for this intelligent responsive system to

display an excellent chemo-photothermal therapy effect.

Evaluation of the biosafety of the mPEG-PAAV micellar system

Biosafety is always a critical concern for nanomedicines applied in the clinic [41]. Thus, a series of *in vivo* experiments were performed to demonstrate that mPEG-PAAV micelles/IR780+DOX would be safe for *in vivo* application. As shown in **Figure S15**, no remarkable changes in behavior or loss of body weight were observed in the mPEG-PAAV/IR780+DOX group during the therapy. Additionally,

to examine whether mPEG-PAAV micelles/IR780+DOX could induce subsequent damage to the major organs, histological analyses were performed after the treatment with different drug formulations. As shown in **Figure 9A**, there was no tissue damage or any other serious side effects in major organs after the systemic administration of mPEG-PAAV/IR780+DOX. However, the H&E images in the free IR780+DOX group showed inflammatory injuries in liver and kidney, such as liver and kidney cell necrosis and inflammatory cell infiltration.

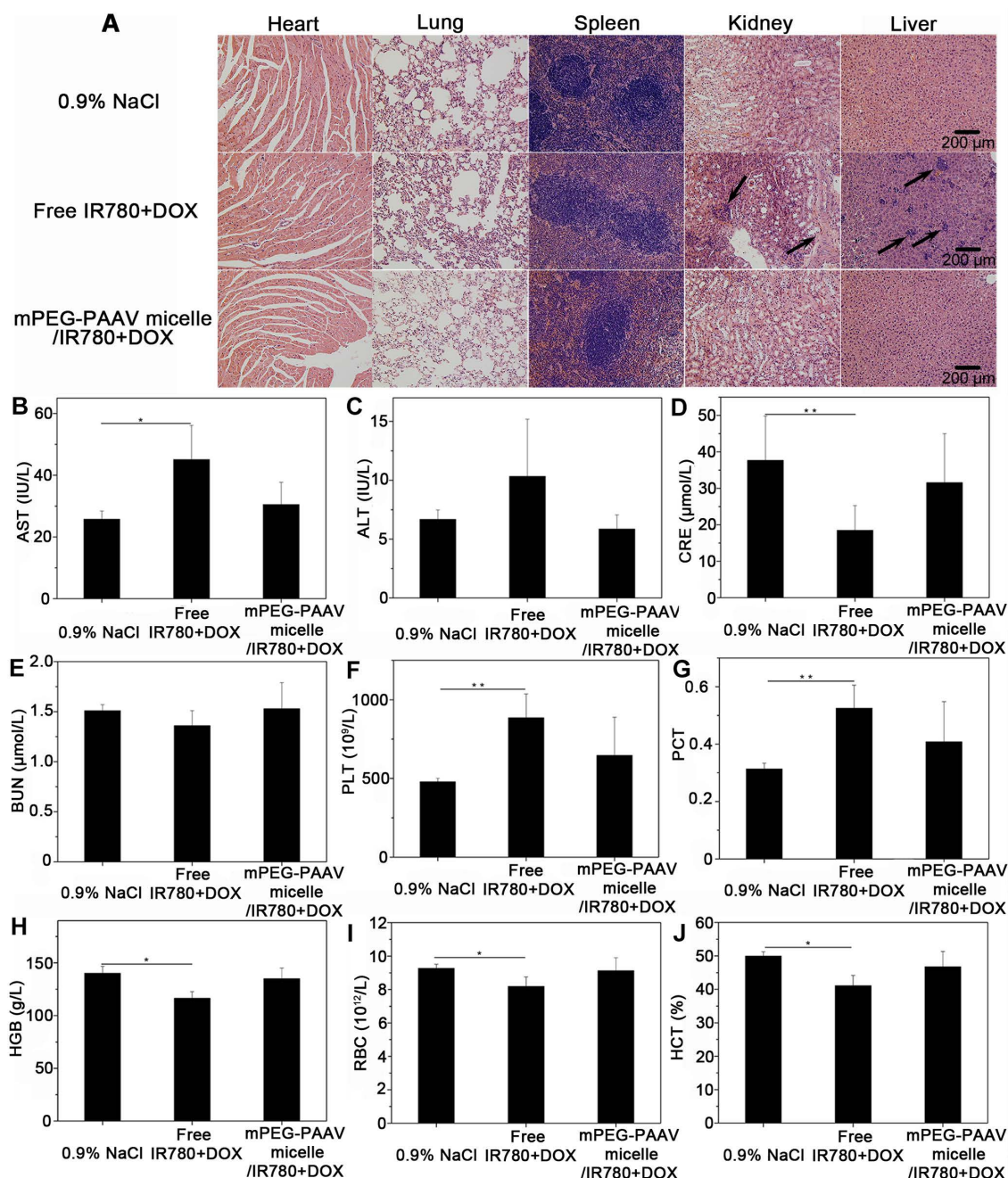


Figure 9. (A) H&E images of the different organs slices from mice on day 29 after the administration of 0.9% NaCl, free IR780+DOX and mPEG-PAAV micelles/IR780+DOX for three times. (B-E) The changes of serum AST, ALT, CRE and BUN levels and (F-J) the routine blood examination on day 29 (n=5).

Additionally, serum biochemistry (AST, ALT, BUN and CRE, which relate to the functions of liver and kidney, respectively) and routine blood tests were conducted to evaluate the long term *in vivo* toxicity [2, 16]. **Figure 9B-E** shows that the levels of AST and CRE in the free IR780+DOX group were significantly different from those in the 0.9% NaCl group. Conversely, the biochemistry results in the mPEG-PAAV micelles/IR780+DOX group were comparable to those in the 0.9% NaCl group, indicating that there was no hepatic or renal dysfunction caused by mPEG-PAAV micelles/IR780+DOX treatment. Additionally, the results of routine blood examination in the mPEG-PAAV micelles/IR780+DOX group also appeared to be normal (**Figure 9F-J** and **Figure S16**). Thus, all these results demonstrate that mPEG-PAAV micelles/IR780+DOX do not cause any obvious side effects for medical use.

Conclusion

In this study, the pH- and thermo-sensitive copolymer (mPEG-PAAV) with UCST was synthesized and employed to prepare a micellar system for delivering IR780 and DOX, which could achieve NIR laser-controlled drug release and PA imaging guidance for chemo-photothermal synergistic therapy. Additionally, the IR780- and DOX-loaded mPEG-PAAV micelles plus NIR laser irradiation could remarkably improve the intracellular accumulation of DOX while synergistically inducing breast cancer cell necrosis, apoptosis, and suppressing migration *in vitro*. More importantly, the treatment with mPEG-PAAV micelles/IR780+DOX plus NIR laser irradiation could completely eliminate the 4T1 breast tumor and thoroughly suppress lung metastasis of breast cancer without displaying any obvious adverse effects in mice. As a whole, these results demonstrate that the hyperthermia-assisted chemotherapy using well-designed IR780- and DOX-loaded mPEG-PAAV micelles presents an effective combined treatment against subcutaneous and metastatic breast tumors.

Abbreviations

CLSM: confocal laser scanning microscope; DOX: doxorubicin; H&E: hematoxylin and eosin; IR780: 2-[2-[2-Chloro-3-[(1,3-dihydro-3,3-dimethyl-1-propyl-2H-indol-2-ylidene) ethylidene]-1-cyclohexen-1-yl]ethenyl]-3,3-dimethyl-1-propylindolium iodide; MTT: methylthiazolyl-diphenyl-tetrazolium bromide; NIR: near-infrared; NMR: nuclear magnetic resonance; OD: optical density; TUNEL: terminal-deoxynucleotidyl-transferase mediated dUTP nick end labelling.

Supplementary Material

Supplementary figures and tables.

<http://www.thno.org/v08p4097s1.pdf>

Acknowledgements

This work was supported by the National Natural Science Foundation of China (51703178, 81770728, 81570655, 51773231), the Postdoctoral Science Foundation of Shaanxi Province (2016BSHED ZZ100), the China Postdoctoral Science Foundation (2015M580855, 2018T111057), the Natural Science Foundation of Shaanxi Province (2018JQ5053), the Fundamental Research Funds for the Central Universities (xjj2016084) and the Natural Science Foundation of Guangdong Province (2016A0303 13315, 2014A030312018, 2014A030313205), Young Teachers Research Funding Program of Sun Yat-Sen University (17ykpy82).

Competing Interests

The authors have declared that no competing interest exists.

References

1. Siegel RL, Miller KD, Jemal A. Cancer statistics, 2016. *CA-Cancer J Clin.* 2016; 66: 7-30.
2. Yang Z, Sun N, Cheng R, et al. Hybrid nanoparticles coated with hyaluronic acid lipid for targeted co-delivery of paclitaxel and curcumin to synergistically eliminate breast cancer stem cells. *J Mater Chem B.* 2017; 5: 6762-75.
3. Minn AJ, Gupta GP, Siegel PM, et al. Genes that mediate breast cancer metastasis to lung. *Nature.* 2005; 436: 518-24.
4. Shi J, Kantoff PW, Wooster R, et al. Cancer nanomedicine: progress, challenges and opportunities. *Nat Rev Cancer.* 2017; 17: 20-37.
5. Wang Y, Xiao Y, Tang RK. Spindle-like polypyrrole hollow nanocapsules as multifunctional platforms for highly effective chemo-photothermal combination therapy of cancer cells *in vivo*. *Chem-Eur J.* 2014; 20: 11826-34.
6. Yan F, Duan WL, Li YK, et al. NIR-laser-controlled drug release from DOX/IR-780-loaded temperature-sensitive-liposomes for chemo-photothermal synergistic tumor therapy. *Theranostics.* 2016; 6: 2337-51.
7. Hahn GM, Braun J, Harkedar I. Thermochemotherapy-synergism between hyperthermia (42-43 degrees) and adriamycin (or bleomycin) in mammalian-cell inactivation. *Proc Natl Acad Sci USA.* 1975; 72: 937-40.
8. Tang Y, Lei TJ, Manchanda R, et al. Simultaneous delivery of chemotherapeutic and thermal-optical agents to cancer cells by a polymeric (PLGA) nanocarrier: an *in vitro* study. *Pharm Res.* 2010; 27: 2242-53.
9. Li ZH, Wang HB, Chen YJ, et al. pH- and NIR light-responsive polymeric prodrug micelles for hyperthermia-assisted site-specific chemotherapy to reverse drug resistance in cancer treatment. *Small.* 2016; 12: 2731-40.
10. Zheng M, Yue C, Ma Y, et al. Single-step assembly of DOX/ICG loaded lipid-polymer nanoparticles for highly effective chemo-photothermal combination therapy. *ACS Nano.* 2013; 7: 2056-67.
11. Chen Q, Liang C, Wang C, et al. An imagable and photothermal "abraxane-like" nanodrug for combination cancer therapy to treat subcutaneous and metastatic breast tumors. *Adv Mater.* 2015; 27: 903-10.
12. Wang C, Xu LG, Liang C, et al. Immunological responses triggered by photothermal therapy with carbon nanotubes in combination with anti-CTLA-4 therapy to inhibit cancer metastasis. *Adv Mater.* 2014; 26: 8154-62.
13. Chen Q, Liang C, Wang X, et al. An albumin-based theranostic nano-agent for dual-modal imaging guided photothermal therapy to inhibit lymphatic metastasis of cancer post surgery. *Biomaterials.* 2014; 35: 9355-62.
14. Torchilin VP. Multifunctional, stimuli-sensitive nanoparticulate systems for drug delivery. *Nat Rev Drug Discov.* 2014; 13: 813-27.
15. Tang S, Meng Q, Sun H, et al. Dual pH-sensitive micelles with charge-switch for controlling cellular uptake and drug release to treat metastatic breast cancer. *Biomaterials.* 2017; 114: 44-53.
16. Yang Z, Sun N, Cheng R, et al. pH multistage responsive micellar system with charge-switch and PEG layer detachment for co-delivery of paclitaxel and curcumin to synergistically eliminate breast cancer stem cells. *Biomaterials.* 2017; 147: 53-67.

17. Li W, Huang L, Ying X, et al. Antitumor drug delivery modulated by a polymeric micelle with an upper critical solution temperature. *Angew Chem Int Ed.* 2015; 54: 3126-31.
18. Li WS, Wang XJ, Zhang S, et al. Mild microwave activated, chemo-thermal combinational tumor therapy based on a targeted, thermal-sensitive and magnetic micelle. *Biomaterials.* 2017; 131: 36-46.
19. Niskanen J, Tenhu H. How to manipulate the upper critical solution temperature (UCST)? *Polym Chem.* 2017; 8: 220-32.
20. Clark EA, Lipson JEG. LCST and UCST behavior in polymer solutions and blends. *Polymer.* 2012; 53: 536-45.
21. Seuring J, Agarwal S. Polymers with upper critical solution temperature in aqueous solution. *Macromol Rapid Comm.* 2012; 33: 1898-920.
22. Hui LW, Qin S, Yang LH. Upper critical solution temperature polymer, photothermal agent, and erythrocyte membrane coating: an unexplored recipe for making drug carriers with spatiotemporally controlled cargo release. *ACS Biomater Sci Eng.* 2016; 2: 2127-32.
23. Yue C, Liu P, Zheng M, et al. IR-780 dye loaded tumor targeting theranostic nanoparticles for NIR imaging and photothermal therapy. *Biomaterials.* 2013; 34: 6853-61.
24. Zhu C, Huo D, Chen Q, et al. A eutectic mixture of natural fatty acids can serve as the gating material for near-infrared-triggered drug release. *Adv Mater.* 2017; 29: 1703702.
25. Shi S, Liu Y, Chen Y, et al. Versatile pH-response micelles with high cell-penetrating helical diblock copolymers for photoacoustic imaging guided synergistic chemo-photothermal therapy. *Theranostics.* 2016; 6: 2170-82.
26. Yang Z, Li Y, Gao J, et al. pH and redox dual-responsive multifunctional gene delivery with enhanced capability of transporting DNA into the nucleus. *Colloids Surf B-Biointerfaces.* 2017; 153: 111-22.
27. Seuring J, Bayer FM, Huber K, et al. Upper critical solution temperature of poly(N-acryloyl glycinamide) in water: a concealed property. *Macromolecules.* 2012; 45: 374-84.
28. Sagle LB, Zhang Y, Litosh VA, et al. Investigating the hydrogen-bonding model of urea denaturation. *J Am Chem Soc.* 2009; 131: 9304-10.
29. Arunkumar P, Indulekha S, Vijayalakshmi S, et al. Synthesis, characterizations, in vitro and in vivo evaluation of etoricoxib-loaded poly (caprolactone) microparticles - a potential intra-articular drug delivery system for the treatment of osteoarthritis. *J Biomat Sci-Polym E.* 2016; 27: 303-16.
30. Jeong JC, Lee J, Cho K. Effects of crystalline microstructure on drug release behavior of poly(epsilon-caprolactone) microspheres. *J Control Release.* 2003; 92: 249-58.
31. Yuan A, Qiu X, Tang X, et al. Self-assembled PEG-IR-780-C13 micelle as a targeting, safe and highly-effective photothermal agent for in vivo imaging and cancer therapy. *Biomaterials.* 2015; 51: 184-93.
32. Engel E, Schraml R, Maisch T, et al. Light-induced decomposition of indocyanine green. *Invest Ophth Vis Sci.* 2008; 49: 1777-83.
33. Park H, Yang J, Lee J, et al. Multifunctional nanoparticles for combined doxorubicin and photothermal treatments. *ACS Nano.* 2009; 3: 2919-26.
34. Meng Z, Wei F, Wang R, et al. NIR-laser-switched in vivo smart nanocapsules for synergic photothermal and chemotherapy of tumors. *Adv Mater.* 2016; 28: 206-53.
35. Yu H, Cui Z, Yu P, et al. pH- and NIR light-responsive micelles with hyperthermia-triggered tumor penetration and cytoplasm drug release to reverse doxorubicin resistance in breast cancer. *Adv Funct Mater.* 2015; 25: 2489-500.
36. Zhu A, Miao K, Deng Y, et al. Dually pH/reduction-responsive vesicles for ultrahigh-contrast fluorescence imaging and thermo-chemotherapy-synergized tumor ablation. *ACS Nano.* 2015; 9: 7874-85.
37. Aggarwal BB, Shishodia S, Takada Y, et al. Curcumin suppresses the paclitaxel-induced nuclear factor-kappa B pathway in breast cancer cells and inhibits lung metastasis of human breast cancer in nude mice. *Clin Cancer Res.* 2005; 11: 7490-8.
38. He X, Bao X, Cao H, et al. Tumor-penetrating nanotherapeutics loading a near-infrared probe inhibit growth and metastasis of breast cancer. *Adv Funct Mater.* 2015; 25: 2831-9.
39. Mallory M, Gogineni E, Jones GC, et al. Therapeutic hyperthermia: the old, the new, and the upcoming. *Crit Rev Oncol Hemat.* 2016; 97: 56-64.
40. Redig AJ, McAllister SS. Breast cancer as a systemic disease: a view of metastasis. *J Intern Med.* 2013; 274: 113-26.
41. Tsang MP, Kikuchi-Uehara E, Sonnemann GW, et al. Evaluating nanotechnology opportunities and risks through integration of life-cycle and risk assessment. *Nat Nanotechnol.* 2017; 12: 734-9.